Design and Test of Innovative Three-Couplers-Based Bandpass Negative Group Delay Active Circuit

Fayu Wan, Taochen Gu, Sebastien Lallechere, Preeti Thakur, Atul Thakur, Wenceslas Rahajandraibe, Blaise Ravelo

Design and Test of Innovative Three Couplers-Based Bandpass Negative Group Delay Active Circuit

Fayu Wan, *Member*, *IEEE*, Taochen Gu, Sébastien Lalléchère, *Member*, *IEEE*, Preeti Thakur, Atul Thakur, Wenceslas Rahajandraibe, *Member, IEEE* and Blaise Ravelo, *Member*, *IEEE*

***Abstract*—An innovative design method of bandpass (BP) negative group delay (NGD) active circuit is developed. The BP NGD topology consists originally of octopole and hexapole coupled line (CL) couplers. The NGD active circuit is validated by a prototype implemented in hybrid technology. The measured results are in good agreement with simulations. The CL-based passive circuit generates BP NGD performance with simulated and measured results showing NGD level of approximately -12 ns having 1.97 GHz center frequency with -11 dB transmission coefficient and -16 dB reflection coefficient. To compensate the loss, active circuit was fabricated by cascading the passive circuit with a microwave amplifier. Subsequently, the previous BP NGD performance is achieved with 0 dB gain. Moreover, a notable active microwave device characterization is performed with the NGD prototype via nonlinear measurements. It was found that the tested NGD prototype operates with 10-dB noise figure, 21 dBm P1dB compression, 29 dBm and 41 dBm OIP3.**

Index Terms— Active topology, Coupled line (CL), Microwave circuit, Bandpass (BP) negative group delay (NGD), Transmission line (TL), Characterization test.

I. INTRODUCTION

THE DELAY effect is one of major roadblocks of communication system performance [1-5]. Nowadays, there is different manifestation of delays. The delay effect can increase the signal distortion. The delay can generate undesired desynchronization between signal data propagating through parallel channels. Among the different delay constraints, the undesirable group delay (GD) effects limit the RF microwave device performances [4-5].

To overcome these undesirable delay effects, different solutions were envisaged by the electronic communication design engineers. Between the developed technique in the literature, the negative group delay (NGD) based compensation technique was expected to be a good solution [6-8]. However, nowadays, the knowledge of NGD function remains limited to very few microwave research design engineers [9-19].

Various tentative fields of application were suggested. For example, circuits operating with bandpass (BP) type NGD function were proposed for designing bilateral gain compensated circuit [9], bidirectional amplifier [20], frequency independent phase shifter [21] and non-Foster element design [22]. However, the BP NGD passive circuits suffer, initially, from excessively high attenuation losses which may reach 20 dB with left-hand metamaterial structures.

To overcome the insertion loss, further research work efforts have been made since early 2010s on the design of microwave NGD active circuits [11-16]. To operate with low attenuation and, significant BP NGD performance, some interesting NGD passive networks [17-19] were introduced. For example, an NGD active circuit implemented with low-noise amplifier (LNA) cascaded with RL- and RC-network based passive circuit was introduced [15-16]. Nonetheless, the lumped component based NGD active circuits are frequency limited. Therefore, some distributed NGD topologies, for example, based on coupled line (CL) based attracted the attention of NGD researchers last decade [17-19]. It is found that the CL based passive BP NGD circuits [17-18] enable to operate with low-loss but not significant NGD figure of merit related to value-bandwidth product. It explains why the microwave engineering is currently facing to the challenge on the design of circuits susceptible to operate with large NGD value and low insertion loss. To face up this technical challenge, one of solutions consists in using RF amplifiers. But this solution raises an obvious question never being solved, until now, about the active microwave circuit constraints such as non-linearity (NL), output 1 dB compression point (P1dB) and noise figure (NF) of BP NGD circuits.

For this reason, the present research work is focused on the design of active and BP NGD circuit including, original

Manuscript received xxx xx, 2020; revised xxx xx, 2020; accepted xxx xx, 2020. Date of publication xxx xx, 2020.

This research work was supported in part by NSFC under Grant 61971230, and in part by Jiangsu Distinguished Professor program and Six Major Talents Summit of Jiangsu Province (2019-DZXX-022) and in part supported by the Startup Foundation for Introducing Talent of NUIST.

Fayu Wan, Taochen Gu, Blaise Ravelo are with the Nanjing University of Information Science & Technology (NUIST), 210044 Nanjing, Jiangsu, China (e-mail: fayu.wan@nuist.edu.cn; 1448661697@qq.com; blaise.ravelo@nuist.edu.cn).

Sébastien Lalléchère is with the Université Clermont Auvergne (UCA), CNRS, SIGMA Clermont, Institut Pascal, Aubière, France. (email: sebastien.lallechere@uca.fr).

Preeti Thakur is with the Department of Physics, Amity University Haryana, India-122413. (email: pthakur@ggn.amity.edu).

Atul Thakur is with the Centre of Nanotechnology, Amity University Haryana, India-122413. (email: athakur1@ggn.amity.edu).

Wenceslas Rahajandraibe are with the Aix-Marseille University, CNRS, University of Toulon, IM2NP UMR7334, Marseille, France (e-mail: wenceslas.rahajandraibe@im2np.fr).

contribution, on NL and NF active circuit characterization. The BP NGD topology under study is comprised of a distributed BP NGD passive circuit cascaded with microwave amplifier. In difference to the existing NGD work [15-16], the present paper is exploring a CL based BP NGD active topology with NL and NF active circuit characterization. The paper is mainly organized in three different sections as follows:

- Section II introduces the design, simulations and experimentations of three CL based passive circuit. The main specifications of the unfamiliar BP NGD function will be introduced.
- Section III focuses on the BP NGD active circuit investigation. After the BP NGD characterizations of the proof of concept, an original study will be performed about the NL and NF aspects. The NGD prototype P1dB, power added efficiency (PAE), NF and third order intercept (IP3) measurement results will be measured and discussed.
- Finally, Section IV is the conclusion.

II. BP NGD Analysis of the Three Coupled Line (CL)-Based Passive Circuit

The present section presents the design of the proof of concept (POC) of the three CL passive circuit in microstrip technology. After the recall on the basic specifications of the unfamiliar BP NGD function. Then, the simulation and measurement results of the BP NGD prototype will be described.

A. Design Description of the Three-CL Based NGD Passive Prototype

As illustrated in Fig. 1(a), the NGD passive schematic under study is originally implemented with combination of two- and three- parallel CLs. As shown in Fig. 1(a), it consists of CLs denoted CL_1 with reference ports (1,3,4,5), CL_2 with reference ports (2,7,9,10) and CL_3 with access ports (4,5,6,7,8,9). $CL_{1,2,3}$ have the same physical lengths, widths, and interspaces. The ports numbered (3,6,8,10) are open ended. This passive structure is a fully distributed circuit without any lossy lumped passive component. Fig. 1(b) and Fig. 1(c) describe the 2-D design and photograph of the fabricated prototype, respectively. This prototype was fabricated on the FR4 substrate whose characteristics are addressed in Table I.

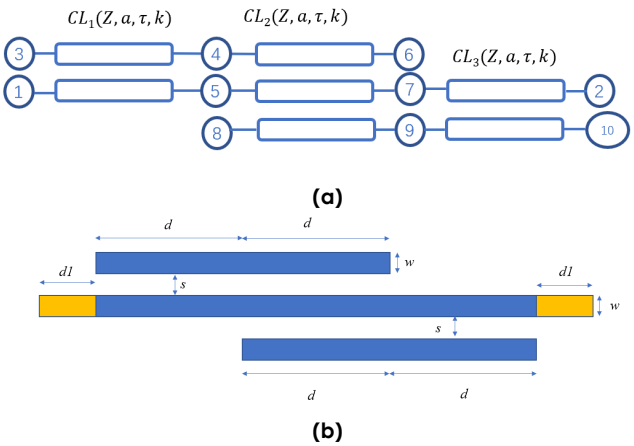

(a)

(b)

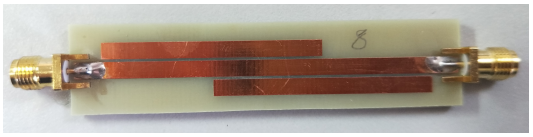

(c)

Fig. 1 (a) Circuit diagram, (b) 2-D design and (c) photograph of the fabricated NGD circuit prototype.

TABLE I
NGD PARAMETERS AND SPECIFICATIONS

Components	*Description*	*Parameter*	*Value*
Dielectric substrate	Material	FR4	-
	Relative permittivity	ε_r	4.4
	Loss tangent	tan(δ)	0.02
	Thickness	h	1.6 mm
Metallization	Material	Copper (Cu)	-
	Thickness	t	35 µm
	Conductivity	σ	58 MS/m
$CL_{1,2,3}$	Length	d	20 mm
	Width	w	3 mm
	Interspace	s	0.5 mm
	Coupling coefficient	k	-11.78 dB
Access line	Length	d_1	5 mm
	Width	w	3 m

Before the fabrication, the CL were slightly optimized in order to reach better NGD performances. The CL physical widths, w, correspond to characteristic impedance, Z=46.6 Ω. The CL quarter wavelength (θ=90°) is set at the NGD center frequency, f_0=1.97 GHz. The considered CLs have the same coupling coefficients, k=−11.78 dB. This fabricated prototype displayed in Fig. 1(c) presents the physical size equal to 20 mm × 90 mm.

Before the exploration of the experimental validation of the three-CL passive circuit prototype, the recall on the unfamiliar BP NGD function specifications will be discussed in the following subsection.

B. Recall on the Frequency Response Parameters for the BP NGD Circuit Analysis

Similar to all microwave circuit, the two-port device analysis was carried out with frequency dependent S-parameters. By denoting the angular frequency variable, $\omega=2\pi f$, acting as symmetric passive topology, the two-dimensional S-matrix model of the CL based circuit can be expressed as:

$$[S(j\omega)]=\begin{bmatrix} S_{11}(j\omega) & S_{12}(j\omega) \\ S_{21}(j\omega) & S_{22}(j\omega) \end{bmatrix}. \quad (1)$$

Acting as a symmetrical circuit, we have the reflection coefficients, $S_{11}(j\omega)=S_{22}(j\omega)$, and transmission coefficients, $S_{21}(j\omega)=S_{12}(j\omega)$. The frequency responses analyses depend on the S-parameter magnitudes:

$$\begin{cases} S_{11}(\omega)=|S_{11}(j\omega)| \\ S_{21}(\omega)=|S_{21}(j\omega)| \end{cases} \quad (2)$$

and also, the transmission phase:

$$\varphi(\omega)=\arg\left[|S_{21}(j\omega)|\right]. \quad (3)$$

From the last expression, we can associate the GD response defined by:

$$GD(\omega) = \frac{-\partial \arg[S_{21}(j\omega)]}{\partial \omega}. \quad (4)$$

The BP NGD analysis consists in identifying a frequency band, $[\omega_1, \omega_2]$, containing the NGD center angular frequency:

$$GD(\omega_0 = 2\pi f_0) = GD_0 < 0, \quad (5)$$

with:

$$GD(\omega_1) = GD(\omega_2) = 0. \quad (6)$$

Meanwhile, when $\omega \in [\omega_1, \omega_2]$, in function of the targeted real value of specifications, *A* and *B*, the BP NGD circuit test should satisfy the following requirement:

$$\begin{cases} GD(\omega) \le 0 \\ S_{21}(\omega) > A \\ S_{11}(\omega) < B \end{cases}. \quad (7)$$

Under these cut-off frequencies, the BP NGD bandwidth is given by:

$$BW = \omega_2 - \omega_1. \quad (8)$$

As practical application of these analytical specifications, NGD analysis of the three-CL passive circuit will be investigated in the following subsection.

C. Discussion on the Three-CL Prototype Simulated and Experimented Results

The simulation results of the three-CL passive circuit were run in the environment of the microwave electronic circuit designer and simulator ADS® Momentum from Keysight Technologies®. All the measurements presented in this work were performed with the vector network analyzer (VNA) from Rohde & Schwarz (ZNB 20, frequency band 100 kHz to 20 GHz).

Figs. 2 display the comparisons of the three CL prototype simulated and measured results. The analyses are performed within the frequency band from 1.9 GHz and 2.05 GHz. As expected, these well-correlated simulated and measured results validate the BP NGD function of the tested microstrip passive circuit. As plotted in Fig. 2(a), at the center frequency, f_0=1.97 GHz, the tested circuit presents the NGD optimal simulated and measurement values, $GD(f_0)$, approximately -11.3 ns against -11 ns, respectively. The NGD bandwidth is approximately 31 MHz.

TABLE II
SIMULATED AND EXPERIMENTED NGD PERFORMANCES OF THE THREE CL-BASED PASSIVE CIRCUIT

Validation Method	f_0 *(GHz)*	GD_n *(ns)*	*BW (MHz)*	S_{21} *(dB)*	S_{11} *(dB)*
Simulation	1.972	-10.3	27	-9.8	-23
Measurement	1.974	-12	31	-11	-16

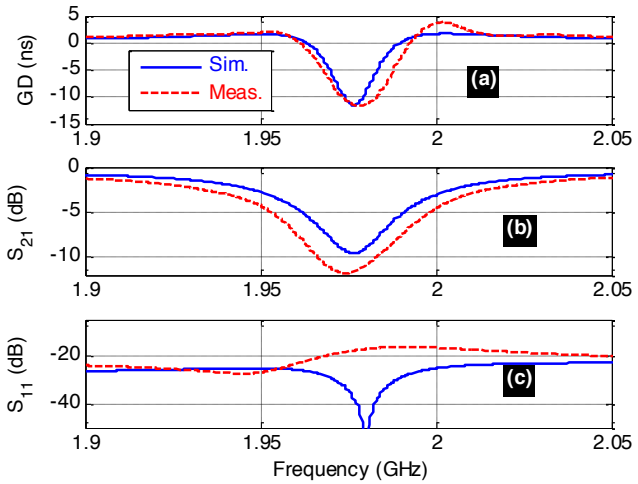

Fig. 2. (a) GD, (b) transmission and (c) reflection coefficients of the fabricated circuit shown in Figs. 1.

As shown in Fig. 2(b) and Fig. 2(c), the transmission coefficient is equal to -11 dB while the reflection coefficient is better than -16 dB within the NGD bandwidth. The differences between the simulated and experimental results are notably due to the numerical computation inaccuracies, the substrate dispersion loss, the metallization skin effect, and the fabricated circuit imperfection in the considered working frequency. Table II summarizes the comparison of NGD performances from the simulation and measurement. We may emphasize that the NGD value and NGD bandwidth are not wide enough for certain applications. The limit of the NGD value induced by the developed three-CL based topology depend on the constituting TL width, length and interspace. Deep analytical investigation about this limitation constitutes the future study. Nevertheless, it can be found that the passive circuit suffers of high attenuation loss.

To overcome this attenuation loss issue, we propose to cascade the circuit with a microwave amplifier. The characterization of BP NGD active prototype will be explored in the following section.

III. BP NGD ANALYSES OF SECOND PROTOTYPE WITH NL AND NF ACTIVE MICROWAVE CIRCUIT CHARACTERIZATION

The present section is focused on the innovative NGD characterization of the designed and fabricated active microwave circuit. The implemented active circuit prototype is designed by combining the previously investigated 3-CL passive circuit with a microwave amplifier. In difference to the existing active NGD circuit investigation [6-16,20-21], the NL and NF of the implemented NGD active circuit prototype are empirically also characterized.

A. BP NGD Validation Test Results of the Second Active Circuit Prototype

To compensate the insertion loss of passive NGD circuit introduced in Figs. 1, we have fabricated another active circuit prototype using a microwave amplifier. In this case, the POC is constituted by passive circuit and a packaged LNA.

1) Design Description and Test Setup of the Active NGD Circuit Prototype

The employed amplifier is a surface mounted monolithic LNA referenced PGA-103+ which is available as a commercial component from mini-circuits® [23]. The schematic of the amplifier including the RLC bias network and DC block networks is introduced in Fig. 3(a). The main parameters implemented in the active circuit prototype are addressed in Table III. Based on the datasheet, the LNA specifications can be represented by its gain, G and reflection, r. In other words, the LNA model can be approximately represented by its equivalent 2-D S-matrix:

$$\left[S_{ampli}(j\omega)\right]=\begin{bmatrix} r & 0 \\ G & r \end{bmatrix}. \quad (8)$$

TABLE III
SPECIFICATIONS OF THE ACCESSORY RLC COMPONENTS FOR BIASING THE MICROWAVE AMPLIFIER

Function	Component	Name	Reference/ manufacturer	Value
DC blocking	Capacitor	*C pass*	Murata	200 pF
Bias network	Resistor	*R*	Murata	100 Ω
	Inductor	*L*	Murata	47 nH
	Capacitor	*C filter*	Murata	100 nF
Amplification	Amplifier	LNA	Mini-circuit (PGA-103+)	-
		G		11dB
		r		20 dB

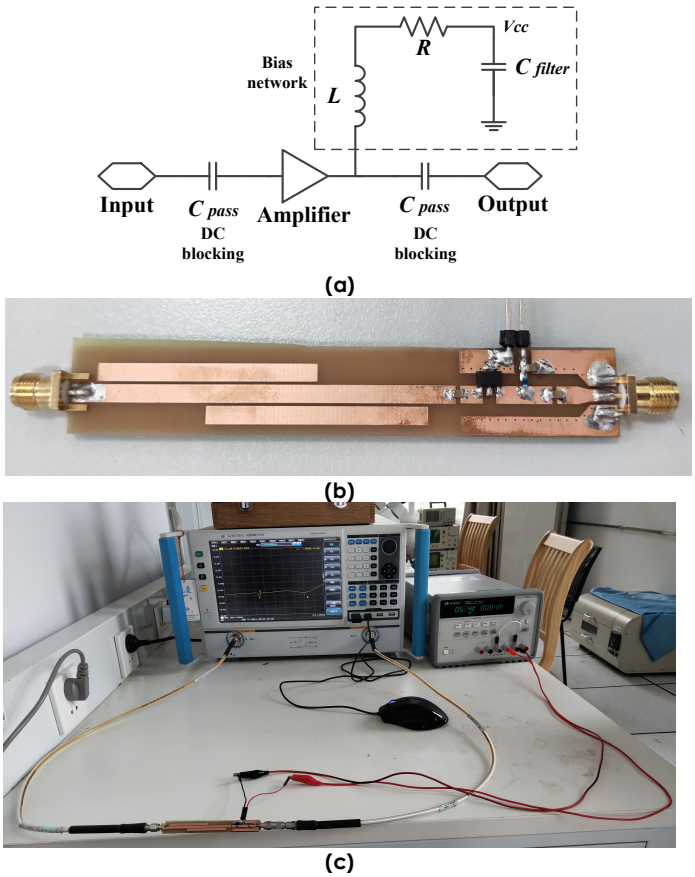

Fig. 3. (a) Schematic of the employed microwave amplifier [23], (b) photograph of the fabricated active NGD circuit. and (c) photograph of the experimental setup.

This table indicates the name, reference, value of LNA, bias networks components, DC block capacitor. Fig. 3(b) introduces the photograph of the fabricated NGD active circuit prototype. It was implemented on the FR4 substrate having specifications indicated previously in Table I. The LNA was inserted in downstream of the passive circuit as defined earlier in the circuit of Fig. 1. As shown in Fig. 3(c), the experimental validation of the BP NGD active circuit prototype was also carried out based-on S-parameter measurements. The test condition was performed by using same VNA as indicated in the last section. During the test, the active circuit was biased with V_0=5 V_{DC} power supply.

2) Discussion on NGD Results of Active Circuit Test

The comparisons between simulation and measurement results are shown in Figs. 4. The S-parameter simulation result of the BP NGD active circuit was generated in the ADS® Momentum environment. During the simulation, the touchstone file of PGA-103+ provided by the manufacturer was considered. The measurement frequency responses are thought in very good correlation with the simulations. Furthermore, the results confirm the BP NGD function without loss expected with the passive NGD circuit combined with a microwave amplifier. It can be pointed up that the amplifier does not influence the GD responses. As shown in Fig. 4(a) and in Fig. 4(b), the NGD performances from measurement and simulations present an excellent agreement on NGD center frequency, value and bandwidth. The relative inaccuracies of reflection coefficient between the measurements and the simulations are better than 5%.

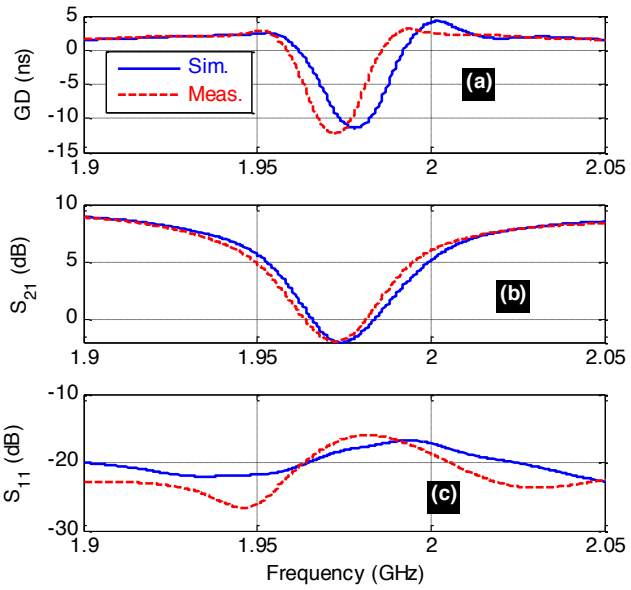

Fig. 4. (a) GD, (b) transmission and (c) reflection coefficients of the fabricated NGD circuit shown in Fig. 3(c).

B. NL and NF Specifications of the Tested BP NGD Active Prototype

In addition to the NGD analyses, the specifications of the tested active circuit were innovatively also assessed. Three different NL and NF major tests of NGD active circuit were

performed. The NL and NF characterization results will be discussed in the following paragraphs.

1) P1dB and PAE Based NGD Active Prototype NL Characterization Test

This NL characterization is based on the simultaneous measurements of the input and output power amplitudes, P_{in} and P_{out}, of the NGD circuit compared to the feeding power, P_{DC}. The NL experimental test setup is highlighted by the diagram of Fig. 5(a). After test, we got the frequency dependent powers, P_{in} and P_{out}. Fig. 5(b) shows the experimental P_{1dB} performance and the *PAE* for active NGD circuit. During the NL test, the bias voltages of the NGD circuit are fixed to V_{GG}= 5 V. From Fig. 5(c), it can be seen that the typical experimental P_{1d}dB is 21.5 dBm at 1.97 GHz. The active NGD circuit power consumption is approximately 420 mW. Then, the PAE is calculated by the equation:

$$PAE = \frac{P_{out} - P_{in}}{P_{dc}} \tag{9}$$

As shown in Fig. 5(b), the tested active NGD circuit PAE is approximately 32%.

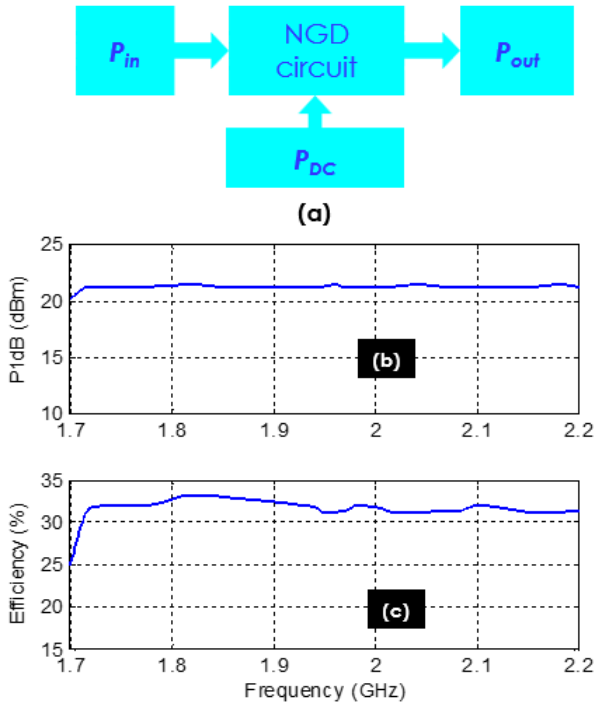

Fig. 5. Experimental results of the NGD active circuit introduced in Fig. 3(b): (a) 1-dB power compression point and (b) PAE.

2) NF Characterization Test of the NGD Active Prototype

The NF characterization of the BP NGD active circuit was carried out as highlighted in Fig. 6(a). It was realized with the EXA signal analyzer N9010A from Agilent Technologies® having frequency band from 10 Hz to 44 GHz. The noise source N4002A is manufactured by Agilent Technologies® operating with frequency band 10 MHz to 26.5 GHz.

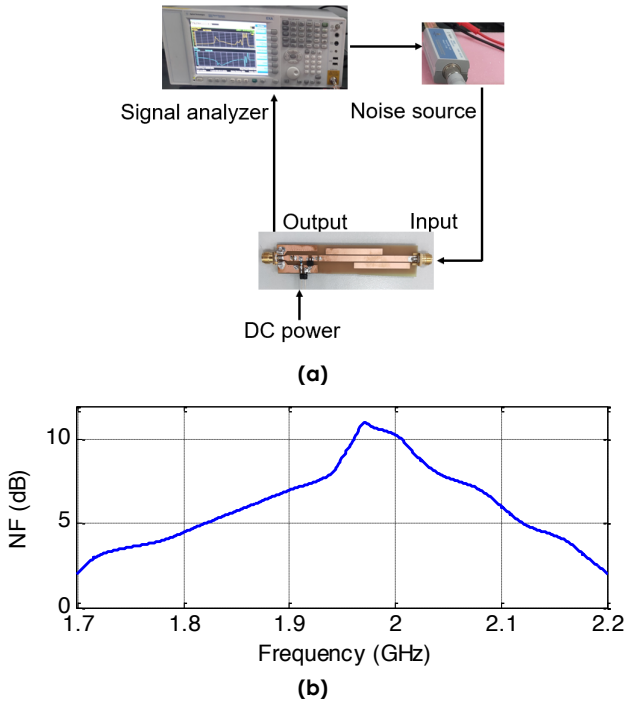

Fig. 6. NF characterization (a) experimental setup and (b) measured result of the NGD active circuit introduced in Fig. 3(b).

The frequency dependent NF result is shown in Fig. 6(b). We emphasize that at 1.97 GHz, the NF achieves its maximum which is approximately 11 dB.

3) IIP3 and OIP3 NL Characterization Test of the NGD Active Prototype

The nonlinearity output third order intercept point (OIP3) and input third order intercept point (IIP3) were measured using the test setup shown in Fig. 7(a). Two signal generators (Agilent MXG Analog Signal Generator N5183A 100 kHz-40 GHz, Agilent N9310A RF Signal Generator 9 kHz-3 GHz) were used to generate two-tone signals with amplitudes, V_1, and V_2, as defined analytically by

$$\begin{cases} v_1(t) = V_1 \sin(2\pi f_1 t) \\ v_2(t) = V_2 \sin(2\pi f_2 t) \end{cases}. \tag{10}$$

By taking, Δf=1 MHz, these harmonic signals are defined by the center frequencies:

$$\begin{cases} f_1 = f_0 \\ f_2 = f_0 + \Delta f \end{cases}. \tag{11}$$

The two-tone signals are combined using the commercial power combiner identified by following reference, ZFRSC-42-S+ operating in the frequency band, DC-4200 MHz from mini-circuits®. The combined signal is visualized with Spectrum analyzer (Agilent MXE EMI Receiver N9038A 20 Hz-26.5 GHz). The two-input signal amplitudes are parametrized with the values. During the test, the fundamental signal is recorded with amplitude P_1. The amplitude of third intermodulation harmonics defined by the relation:

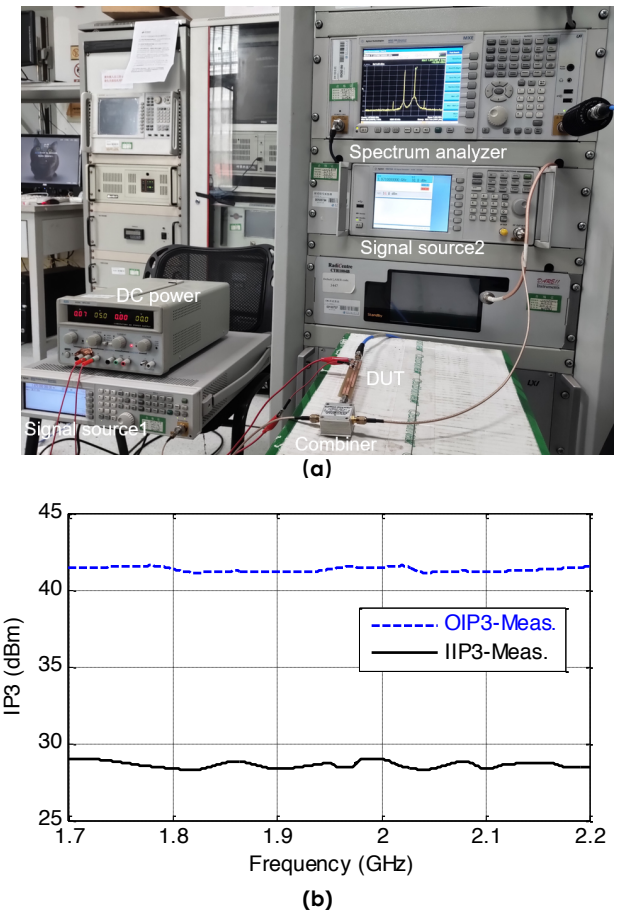

Fig. 7. OIP3 and IIP3 characterization (a) experimental setup and (b) measured results.

$$f_h = 2f_1 - f_2 \tag{12}$$

is recorded as P_2. The OIP3 is calculated by:

$$OIP3 = \frac{P_1 - P_2}{2} + P_1 . \tag{13}$$

The IIP3 is calculated by the equation:

$$IIP3 = OIP3 - gain. \tag{14}$$

The frequency dependent measured OIP3 and IIP3 are plotted in Fig. 7(b). It can be pointed out from this test result that the OIP3 is 41 dBm and the IIP3 is 29 dBm.

C. Discussion on the Active Prototype Performances Compared with the Literature

One may wonder about the performances of the tested NGD active circuit with respect to the existing ones in the literature. This last subsection proposes a brief comparative study with respect to the existing work.

1) Discussion on NGD Performances

The comparisons of the proposed BP NGD performance with the exiting results in the literature [12, 14-15] are summarized in Table IV. It is noteworthy that compared to the previous work, the introduced passive and LNA-based NGD topology shows notable advantages in terms of possibility to operate with large NGD value, high center frequency, design simplicity and good non linearity characteristics, large P1dB point and low noise figure. The designed NGD active prototype has a better NGD performance and figure-of-merit (FoM), which is defined as:

$$FoM = \left|GD(f_0)\right| \times BW \times \left|S_{21}(f_0)\right|. \tag{15}$$

TABLE IV
NGD PERFORMANCE COMPARISON

References	f_0 (GHz)	GD_n (ns)	BW (MHz)	S_{21} (dB)	FoM
[12]	1	-1	200	0	0.2
[14]	1.15	-3	75.9	0	0.22
[15]	0	-5	32	0	0.16
This work	1.97	-12	31	-0.5	0.35

2) Discussion on the NL and NF Performances with Respect to GSM, UMTS and 5G Devices

The NL parameters such as 1 dB gain compression point, NF and the third-order intercept points are the main parameters for the active microwave device performances. Among the most critical devices, we can consider the amplifier and mixer device NL in order to define the dynamic range of their operation. These parameters can be connected to adjacent channel power ratio and error vector magnitude (EVM) in amplifiers and must be kept under control. Thus, the GSM UMTS and 5G communication all have guidelines on the PAE, NF and OIP3. As shown in Table V, this work presents better PAE and OIP3 performances than the requirement of wireless communication.

TABLE V
COMPARISON OF NL AND NF CHARACTERISTIC PERFORMANCES

References	*PAE*	*NF* (dB)	*OIP3* (dBm)
GSM	20%	10	35
UMTS	20%	9.6	32
5G	15%	-0.5	35
This work	32%	11	41

IV. CONCLUSION

An original test characterization of active circuit exhibiting BP NGD function is investigated. The BP NGD circuit is tested for the characterization based on NL and NF measurements.

The NGD prototype consists of CL based passive circuit cascaded with microwave amplifier. The designability of the innovative BP NGD topology is confirmed with simulations and measurements of microstrip distributed circuit-based prototype. As expected, the feasibility of loss compensation was verified under about 10-dB NF added with measurements of P1dB, PAE, IIP3 and OIP3. The measured NF and NL performances of the innovative active BP NGD circuit are rather good enough for certain cases of RF and microwave devices.

In the continuation of the present research work, the improvement of different NGD circuit performances are in progress. Doing this, the design with the proposed BP NGD passive topology can be improved as follows. To increase the NGD bandwidth, passive cells targeted to operate at slightly different NGD center frequencies can be associated in cascade. To reduce the size, we can modify the shape of constituting conductor line constituting the NGD circuit instead of using straight I-line.

The performance of the tested prototype is encouraging for the development of BP NGD active circuit for future RF and

microwave systems as 5G devices.

REFERENCES

[1] E. C. Heyde, "Theoretical Methodology for Describing Active and Passive Recirculating Delay Line Systems," Electronics Letters, Vol. 31, No. 23, Nov. 1995, pp. 2038-2039.

[2] C. Wijenayake, Y. Xu, A. Madanayake, L. Belostotski and L. T. Bruton, "RF Analog Beamforming Fan Filters Using CMOS All-Pass Time Delay Approximations," IEEE Trans. CAS I: Regular Papers, Vol. 59, No. 5, May 2012, pp. 1061-1073.

[3] M-E. Hwang, S-O. Jung and K. Roy, "Slope Interconnect Effort: Gate-Interconnect Interdependent Delay Modeling for Early CMOS Circuit Simulation," IEEE Trans. CAS I, Vol. 56, No. 7, Jul. 2009, pp. 1428-1441.

[4] S.-S. Myoung, B.-S. Kwon, Y.-H. Kim and J.-G. Yook, "Effect of group delay in RF BPF on impulse radio systems," IEICE Trans. on Communications, vol. 90, no. 12, pp. 3514-3522, 2007.

[5] G. Groenewold, "Noise and Group Delay in Active Filters," IEEE Trans. CAS I: Regular Papers, Vol. 54, No. 7, July 2007, pp. 1471-1480.

[6] B. Ravelo, "Neutralization of LC- and RC-Effects with Left-Handed and NGD Circuits", Advanced Electromagnetics (AEM), Vol. 2, No. 1, Sept. 2013, pp. 73-84.

[7] B. Ravelo, "Recovery of Microwave-Digital Signal Integrity with NGD Circuits", Photonics and Optoelectronics (P&O), Vol. 2, No. 1, Jan. 2013, pp. 8-16.

[8] B. Ravelo, S. Lalléchère, A. Thakur, A. Saini and P. Thakur, "Theory and circuit modelling of baseband and modulated signal delay compensations with low- and band-pass NGD effects", Int. J. Electron. Commun. (AEÜ), Ed. Elsevier, Vol. 70, No. 9, Sept. 2016, pp. 1122–1127.

[9] M. Kandic and G. E. Bridges, "Bilateral Gain-Compensated Negative Group Delay Circuit," IEEE Microwave and Wireless Components Letters, Vol. 21, No. 6, May 2011, pp. 308-310.

[10] M. Zhu and C. M. Wu, "A Tunable Non-Foster T-Network Loaded Transmission Line Using Distributed Amplifier-Based Reconfigurable Negative Group Delay Circuit," in Proc. 2018 Asia-Pacific Microwave Conference (APMC), Kyoto, Japan, 6-9 Nov. 2018, pp. 720-722.

[11] C.-T. M. Wu, S. Gharavi, B. Daneshrad, and T. Itoh, "A dual-purpose reconfigurable negative group delay circuit based on distributed amplifiers," IEEE Microw. Wireless Compon. Lett., vol. 23, no.11, pp. 593-595, Nov. 2013.

[12] C.-T.-M. Wu and T. Itoh, "Maximally flat negative group-delay circuit: A microwave transversal filter approach," IEEE Trans. Microw. Theory Techn., vol. 62, no. 6, pp. 1330-1342, Jun. 2014.

[13] T. Zhang, T. Yang and P. L. Chi, "Novel Reconfigurable Negative Group Delay Circuits With Independent Group Delay and Transmission Loss/Gain Control," IEEE Trans. Microw. Theory Techn., vol. 68, no. 4, pp. 1293-1303, Apr. 2020.

[14] M. Kandic, and G. E. Bridges, "Asymptotic limits of negative group delay in active resonator-based distributed circuits," IEEE Trans. Circuits and Systems I: Regular Papers, vol. 58, no. 8, pp. 1727-1735, 2011.

[15] F. Wan, N. Li, B. Ravelo, Q. Ji, B. Li, and J. Ge, "The design method of the active negative group delay circuits based on a microwave amplifier and an RL-series network," IEEE Access, vol. 6, pp. 33849-33858, Jun. 2018.

[16] F. Wan, N. Li, B. Ravelo, J. Ge, and B. Li, "Time Domain Experimentation of NGD Active RC-Network Cell," IEEE Trans. Circuits and Systems II, vol. 66, no. 4, 2019, pp.562-566.

[17] G. Chaudhary and Y. Jeong, "Low signal-attenuation negative group-delay network topologies using coupled lines," IEEE Trans. Microw. Theory Techn., vol. 62, no. 10, pp. 2316-2324, Oct. 2014.

[18] G. Chaudhary and Y. Jeong, "Transmission-type negative group delay networks using coupled line doublet structure," IET Microw., Antennas Propag., vol. 9, no. 8, pp. 748-754, Jun. 2015.

[19] Y. Wu, H. Wang, Z. Zhuang, Y. Liu and Q. Xue, "A Novel Arbitrary Terminated Unequal Coupler With Bandwidth-Enhanced Positive and Negative Group Delay Characteristics," IEEE Trans. Microw. Theory Techn., vol. 66, no. 5, pp. 2170-2184, May 2018.

[20] Y. Meng, Z. Wang, S. Fang, T. Shao and H. Liu, "A Broadband Switch-Less Bi-Directional Amplifier with Negative-Group-Delay Matching Circuits," Electronics, vol. 7, no. 158, pp. 1-11, Aug. 2018.

[21] B. Ravelo, "Distributed NGD active circuit for RF-microwave communication," Int. J. Electron. Commun., vol. 68, no. 4, pp. 282-290, Apr. 2014.

[22] T. Zhang, R. Xu and C. M. Wu, "Unconditionally Stable Non-Foster Element Using Active Transversal-Filter-Based Negative Group Delay Circuit," IEEE Microw. Wireless Compon. Lett., vol. 27, no. 10, pp. 921-923, Oct. 2017.

[23] Available Online, https://www.minicircuits.com/WebStore/dashboard.html?model=PGA